JOURNAL OF CATALYSIS 137, 114–126 (1992)

An XPS Study of Interactions in Thin Films Containing a Noble Metal with Valence-Invariant and Reducible Oxides

M. SHELEF, L. P. HAACK, R. E. SOLTIS, J. E. DEVRIES, AND E. M. LOGOTHETIS

Ford Motor Company, Research Staff, Dearborn, Michigan 48121

Received August 19, 1991; revised March 27, 1992

X-ray photoelectron spectroscopy was employed to examine the reducibility of oxides possessing multiple oxidation states (titania, niobia, and ceria) in the presence of palladium and a valence-invariant oxide (lanthana). The materials consisted of sputter-deposited ultra-thin films containing palladium with either titania, niobia, or ceria, with and without lanthana, on a sapphire substrate. For lanthana/palladium films, no reduction of the lanthana surface was observed after *in situ* treatment in hydrogen up to 600°C. After similar treatment, in the absence of lanthana a partial reduction to the lower oxidation states of niobia and titania and a total reduction to the lower oxidation state of ceria was observed. The presence of lanthana in the films inhibits the reduction of the titania completely and that of the niobia and ceria partially. Also, in a complementing set of films containing ceria an overlayer of high-surface-area γ-Al_2O_3, from the decomposition of an aqueous film of aluminum propoxide, was put over the smooth sapphire surface before the deposition of the other film components. In this case, the inhibiting effect on ceria-reducibility was attenuated. This points to the redistribution of lanthana over the available oxide surfaces. The preponderant portion of the lanthana accommodated on the porous γ-Al_2O_3 has rendered a significant part of the ceria unprotected and, in the presence of Pd, susceptible to reduction by H_2 at 600°C. The results of these studies are a further manifestation of the known surface reactivity of lanthana, which while remaining itself irreducible, may strongly affect the behavior of other irreducible oxides such as alumina, or as presently shown, of reducible oxides such as titania, niobia, and ceria. © 1992 Academic Press, Inc.

INTRODUCTION

The interaction of noble metals with oxide promoters and supports has been a major topic of study in the last ten years or so. It has been well established that these interactions, termed "strong" to denote the formation of what in the broad sense may be considered chemical bonding, take place when the oxide support or promoter is reducible (*1*). An example of this type of interaction involved the support titania, where titanium possesses two accessible oxidation states (+2, +4).

In the last 5 years there has also been a series of publications, some of them referenced in the above-mentioned review (*1*), illustrating that strong interactions can take place as well when noble metals are supported on oxides, such as lanthana, in which multiple oxidation states are not accessible. These exceptions have been observed under conditions not easily induced under laboratory conditions (*2, 3*). Thus, contrary to the previously accepted view (*4*), this "strong" interaction did not correlate with the bulk reducibility of the oxides.

The distinction between the behavior of dual oxidation state oxides (e.g., titania) and that of the valence-invariant ones (e.g., lanthana), where the only accessible oxidation state La^{3+} is isoelectronic with xenon, is unclear. This was evident in the conclusions of Rieck and Bell (*5*), where a completely analogous behavior of lanthana and titania was noted in promoting and modifying the catalytic activity of Pd under reducing conditions.

The interest in lanthana (and other valence-invariant rare earth oxides) was precipitated by observation of unexpected catalytic behavior when lanthana was pres-

0021-9517/92 $5.00
Copyright © 1992 by Academic Press, Inc.
All rights of reproduction in any form reserved.

ent. Enhanced activity in the reduction of nitric oxide was noted by Muraki *et al.* (*6, 7*). In the hydrogenation of carbon monoxide, the addition of lanthana to silica-supported noble metal catalysts had a very marked effect on the course of reaction (*8*). Even pure lanthana was observed to abstract hydrogen atoms from methane, producing gaseous methyl radicals (*9*). In the intervening years there were subsequent publications on these observations. It is these potentially important implications that led to our study of the interaction of noble metals with the lanthana support.

As noted above, we became aware of a series of previous efforts to produce oxygen-deficient phases in valence-invariant rare earth oxides (*10*). These phases were attained by either reduction in hydrogen at 1400°C, smelting, or heating of the oxides with corresponding hydrides (or metals) at temperatures exceeding 2000°C. In the case of lanthana, a slight reduction of the oxide was observed at 1400°C in an La_2O_3–La system (*11*).

The purpose of this paper is to present XPS results confirming the irreducibility of lanthana under more commonly obtainable conditions and, under the same conditions, characterize the interaction of this oxide with reducible oxides (Ti, Nb, Ce) in the presence of a noble metal (Pd). The studies involved the characterization of thin films containing these oxides sputter-deposited onto sapphire. The rationale for using titania and niobia for the reducible oxides is that they possess easily accessible lower oxidation states. Ce was studied for its role in automotive catalyst systems. Although normally used as an oxygen-storage component (*12–15*), when oxygen-deficient it also can be an active catalyst for other reactions. Just recently, an enhanced storage capacity was claimed in $CeO_2/La_2O_3/Al_2O_3$ powders in contact with precious metals (*16*).

Finally, a quartenary film consisting of a noble metal (Pd), a reducible multivalent oxide (ceria), a valence-invariant oxide (lanthana), and γ-Al_2O_3 (deposited first on the sapphire) was investigated to establish whether partitioning of the valence-invariant oxide would occur in the film between high-surface-area γ-Al_2O_3 and ceria if both were present. Alumina, as γ-Al_2O_3, is also valence-invariant, but it is less reactive, i.e., with respect to CO_2 and H_2O, and its surface is less basic than that of lanthana. High-surface-area γ-Al_2O_3 has a high affinity for La (*17*) and therefore should adsorb the lanthana from the overlying film.

EXPERIMENTAL

Standards

Lanthanum chloride anhydrous ($LaCl_3$) and high purity (99.99$^+$%) Pd foil were obtained from Alfa Products. A reference for PdO was obtained by oxidizing the Pd foil *in situ* at 300°C in O_2 for 1 h.

Preparation of Films on Sapphire

Ultra-thin films were prepared by RF sputter-deposition utilizing a commercial diode sputtering unit. The unit was a Perkin–Elmer Randex model 2400 three-source RF sputtering system. The films were deposited onto $10\bar{1}0$ sapphire substrates polished to an optical smoothness and measuring 1 cm × 1 cm × 0.05 cm. The substrates were situated on a rotating table approximately 5 cm away from the targets. The rate of rotation could be varied over a wide range to control the time that a substrate spends under a given target.

The sapphire substrates were cleaned prior to deposition in soapy water and then rinsed in an ultrasonic cleaner in deionized water followed by isopropyl alcohol. The substrates were loaded into the sputtering system which was evacuated to a pressure of 1×10^{-7} Torr. Ultra-high-purity argon gas was bled into the system at a constant rate to attain a pressure of 4 mTorr. Prior to film deposition the substrates were sputter-cleaned *in situ* to remove any remaining surface contamination.

La/Pd films. The Pd and La metal source targets (99.9% purity) used were supplied by Perkin–Elmer, Ultek Div, and Pure Tech,

Inc., respectively. The sputtering rates of the individual Pd and La targets had been previously calibrated using sapphire substrates which were masked to determine final film thickness.

Films containing Ti and Nb. These films contained Pd, with and without La, with either TiO_2 or Nb_2O_5. The TiO_2 and Nb_2O_5 source targets (99.9 and 99.95% pure, respectively) were supplied by Cerac, Inc., and KEMA, respectively. The sputter-deposition rates of the oxide materials were calibrated in the same manner as for the Pd and La metals.

The two binary films produced consisted of 10 Å of the reducible oxide (Ti or Nb) under 5 Å of Pd. The ternary films consisted of Pd deposited directly over the valence-invariant oxide (La), with the reducible oxide (Ti or Nb) deposited previously on the sapphire substrate or last on the topmost surface. The sequential differences provided information on the effect of the sputtering order on the reducibility of the film components.

Films containing Ce. These films on sapphire contained Pd and Ce oxide also with and without La. The CeO_2 source target (99.9% purity) was supplied by Cerac, Inc. The sputter-deposition rate for Ce oxide was calibrated in the same manner as for the other materials.

To provide the high-surface-area γ-Al_2O_3, some of the substrate sapphire slides were dipped, while in a glove box under a nitrogen atmosphere, into a solution containing 100 mg $Al(C_3H_7O)_3$ (aluminum isopropoxide) in 30 ml of isopropyl alcohol. The excess solution was run-off the vertically held slides and then, after drying, the coated slides were exposed to the air. Upon heating to 600°C in air for several hours, a film of γ-Al_2O_3 was assumed to be formed. The aim was to make a film ~0.1 μm (1000 Å) thick or less. A reliable measure of the film thickness was not made, however, the exact thickness of the film of γ-Al_2O_3 is of little consequence, provided it is sufficiently thick to accommodate the spreading of lanthana.

It was decided to keep constant the amount of ceria (10 Å thickness) and also the sequence of deposition, ceria first, then palladium, followed by lanthanum. The two variables to be studied were (a) the amount of lanthana required to impede the reduction of the ceria and (b) the effect of the presence of the γ-Al_2O_3 underlayer. A Pd/CeO_2 film was also produced as a reference material.

Typical deposition rates were 145 Å/min using 50 W incident RF power for the Pd metal and 150 Å/min with 100 W incident RF power for the La metal. Due to the rapid oxidation of the La metal target when the system was opened to air, it was necessary to presputter this target for several hours to remove the oxide layer prior to film deposition. After presputtering for 4 h using 150 W RF power, the oxide layer was effectively removed and a constant sputtering rate was achieved.

Once the stationary sputtering rates had been established for each target, ultra-thin films (equivalent thickness of less than 20 Å) could be fabricated by rotating a substrate under the desired target for a specified time. Films containing a combination of metals could be fabricated by successively rotating the substrate under each target for the appropriate time. After deposition, the samples were removed and stored under argon.

Table 1 summarizes the sequence of the depositions and the nominal thickness of each film component in these materials. The left-to-right order in this table beginning with the sapphire substrate denotes the film deposition sequence. The components of each film are designated by the targets from which they were sputtered. The oxygen stoichiometry of the films as prepared was not determined.

X-ray Photoelectron Spectroscopy Measurements

The analyses were performed using an M-Probe XPS spectrometer manufactured by Surface Science Instruments (VG-Fisons), Mountain View, CA. The X-ray source utilized monochromatic Al$K\alpha$

TABLE 1

Compositional Makeup of Sputter-Deposited Films

Sample	Layer thickness (Å)
1	Sapphire/10 La/5 Pd
2	Sapphire/5 Pd/10 La
3	Sapphire/10 TiO_x/5 Pd
4	Sapphire/5 TiO_x/5 La/5 Pd
5	Sapphire/10 La/5 Pd/5 TiO_x
6	Sapphire/10 NbO_x/5 Pd
7	Sapphire/5 NbO_x/5 La/5 Pd
8	Sapphire/10 La/5 Pd/5 NbO_x
9	Sapphire/10 CeO_x/5 Pd
10	Sapphire/10 CeO_x/5 Pd/5 La
11	Sapphire/10 CeO_x/5 Pd/10 La
12	Sapphire/10 CeO_x/5 Pd/20 La
13	Sapphire/γ-Al_2O_3/10 CeO_x/5 Pd/10 La
14	Sapphire/γ-Al_2O_3/10 CeO_x/5 Pd/20 La

(1486.6 eV) radiation focused to a 600-μm diameter beam. The incident X-ray radiation and take-off angle of the electrons analyzed were fixed at 35° for all acquisitions. The base pressure of the spectrometer analyzer was 5×10^{-10} Torr. The analyzer was operated with a 150-eV pass energy for acquisition of survey spectra for quantification, and a 50-eV pass energy for acquisition of high-resolution core-level spectra. An electron flood gun in conjunction with a charge neutralization screen was used to minimize any surface charging effects. The effectiveness of these, in concert, to circumvent charging effects has been thoroughly discussed elsewhere (*18*). In addition, ancillary experiments were also undertaken to define if any differential charging existed utilizing the acquisition parameters described. These experiments consisted of varying the energy and flux of charge neutralization electrons impinging on the surface of the sample and observing any differences in the binding energy separation of the Al from the main peak envelopes of the metal and metal oxide film constituents. No differences in separation were noted and only minimal distortion of each respective peak was observed, suggesting that appreciable differential charging had not occurred.

The data system used was also supplied by same vendor. Quantification of survey data was done by routines based on the Scofield photoionization cross-section values. High-resolution core-level spectra were peak-fitted using a least-squares fitting routine to accurately determine binding energy positions, component intensities, and full width at half maximum (FWHM). In the case of lanthanum, the peak positions were determined for both the core and satellite lines. The high resolution Ti $2p$ and Nb $3d$ spectra presented in this paper represents the spectra of the Ti $2p_{3/2}$, $2p_{1/2}$ and Nb $3d_{5/2}$, $3d_{3/2}$ spin–orbit splittings, respectively. Therefore each chemical state of Ti and Nb will exist as two peaks in the high-resolution spectra acquired. To increase the confidence in the computer fit of spectra with multiple states, the spin–orbit spectral envelope may be fit as a single envelope knowing the binding energy separation and the intensity ratio. The separation and intensity ratio of the splitting has been empirically derived and agrees well with theoretical values. Therefore these values were held as fixed constants in the fitting routines and only the spectral position, FWHM, and intensity of each complete envelope were allowed to iterate freely within the program. Only the Ti $2p_{3/2}$ and Nb $3d_{5/2}$ binding energies are reported in this work. In the case where Ce was present as a combination of Ce^{4+} and Ce^{3+} states, the least-squares fitting routine was used to accurately determine the area of the u''' peak of Ce^{4+}, which resided over a small and broad peak associated with the $3d_{5/2}$ core level of Ce^{3+}.

Core-level spectra of insulating species were referenced either to the sapphire substrate Al $2p$ line at 73.9 eV, or when the γ-Al_2O_3 layer was present to the Al $2p$ line at 74.2 eV. Conducting species were referenced to the Fermi edge. All binding energy positions measured were accurate to ± 0.2 eV.

A PHI Model 04-800 Reactor System was mounted onto the sample preparation chamber the M-Probe spectrometer. The base pressure of the sample preparation chamber

was 1×10^{-9} Torr. The base pressure of the reactor was 5×10^{-8} Torr. The reactor gases used were Ar (99.9995%0), O_2 (99.98%), and H_2 (99.9995%), purchased from Matheson. The treatments were carried out in 1 atm of gas at 600°C for 19 h (overnight) using a flow rate of ≈100 cm^3/min. In the case of Ti- and Nb-containing films, a second reduction treatment was performed for 48 h under the same flow and temperature conditions. Immediately following every treatment samples were transferred directly from the reactor to the analyzer *in vacuo* to eliminate contamination due to air exposure. XPS analyses were acquired on all samples as received and after each treatment.

RESULTS

The thin films were chosen as a model to assure intimate contact between the noble metal, the valence-invariant oxide, and the reducible oxide, and to increase the likelihood of interpenetration of both oxides with the noble metal when subjected to *in situ* oxidative and reductive treatments.

XPS Quantitative Results

The films "as received" contained significant amounts of carbon contamination (50–70%). Most of the carbon was attributed to an adventitious overlayer, but when La was present, the air-exposed films also contained lanthanum carbonates (*17*). No detectable C was observed after the oxidative treatment, however, 5–10% C reappeared after the reductive treatments. In the case of Ti- and Nb-containing films, the quantitative results of the materials after the 4- and 48-h reductions were essentially identical. In addition, core-level data were identical for these reductions as well. These results suggest that a steady state was achieved after the 4-h reduction. The compositional data for each of the films were not included in this paper. To more appropriately assess the distribution of the film constituents with respect to lanthana, initially and after each successive chemical treatment, the La/Pd and La/metal-oxide ratios were tabulated for each series of experiments and are presented in Table 2. This ratio is independent of the presence of adventitious contamination (mostly observed on the as received surfaces). The La ratios of Table 2 will be discussed later along with the representative core level data.

Small amounts of Cl and Si were present in the films after the initial sputter-deposition. The initial *in situ* oxidative treatment removed the Cl and Si, but deposited trace amounts of Zn, S, Na, K, and Mo. The following reductive treatment removed S, but small amounts of Cl reappeared. Except for the observed chemical states for the highly reactive La, the effects any amount of S or Cl exhibited towards the chemistry and reducibility of components in these films are believed to be negligible. This point is discussed further in the next section.

Binding Energies/Oxidation States

Due to the effects of contamination on the initially sputter-deposited metals (adventitious carbon, metal hydroxides, carbonates, chlorides, etc.), except for the preliminary La/Pd films, only core-level spectra acquired after *in situ* oxidative and reductive treatments are presented. Also the La and Pd core-level spectra, although acquired for all films containing La and Pd included in this study, are only given for the La/Pd films.

La/Pd films. The La and Pd core level spectra are shown only for sample 1, since the spectra observed for sample 2, which differed only in deposition sequence, were identical. Comparison of the Pd states observed on the as-received material to those observed after reactor treatments is given in Fig. 1. The Pd $3d_{5/2}$ binding energy of the major constituent for the as-received material (334.9 eV) is consistent with that observed for metallic Pd foil (335.2 eV). After treatment in O_2 at 600°C, the Pd binding energy is observed at 336.6 eV, identical to that observed for a reference PdO foil. Upon

TABLE 2

La/Pd and La/Metal–Oxide Ratios as a Function of Treatment

	Sample	Atomic ratio							
		La/Pd				La/metal oxide			
		Init.	O_2	H_2	O_2	Init.	O_2	H_2	O_2
1	(10 La/5 Pd)	0.79	0.66	0.78					
2	(5 Pd/10 La)	1.3	0.74	0.72					
4	(5 TiO_x/5 La/5 Pd)	0.05	0.12	0.25		0.61	1.3	1.6	
5	(10 La/5 Pd/5 TiO_x)	0.24	0.31	0.66		0.48	1.4	2.8	
7	(5 NbO_x/5 La/5 Pd)	0.17	0.31	0.65		0.96	1.4	1.3	
8	(10 La/5 Pd/5 NbO_x)	0.56	0.70	1.0		0.69	1.6	1.8	
10	(10 CeO_x/5 Pd/5 La)	0.91	0.86	0.85	0.97	8.6	12	2.5	4.5
11	(10 CeO_x/5 Pd/10 La)	1.2	0.94	0.91	0.92	10	7.5	2.6	4.8
12	(10 CeO_x/5 Pd/20 La)	3.7	2.6	2.4	1.9	14	35	8.3	11
13	(γ-Al_2O_3/10 CeO_x/5 Pd/10 La)	0.9	0.9	1.0	0.9	3.9	3.2	1.1	1.9
14	(γ-Al_2O_3/10 CeO_x/5 Pd/20 La)	2.5	2.4	2.6	1.5	8.4	6.4	2.0	4.6

reduction in H_2, Pd in the La/Pd film is reduced entirely to the metallic state (Pd $3d_{5/2}$ binding energy at 335.0 eV). These results are consistent with those observed for bulk Pd when supported on γ-Al_2O_3 (*19*).

As to the oxidation state of lanthanum, Fig. 2 shows that initially the La $3d_{5/2}$ peak binding energy was observed at 835.0 eV. The satellite peak 3.7 eV higher in binding energy was greater in intensity than the

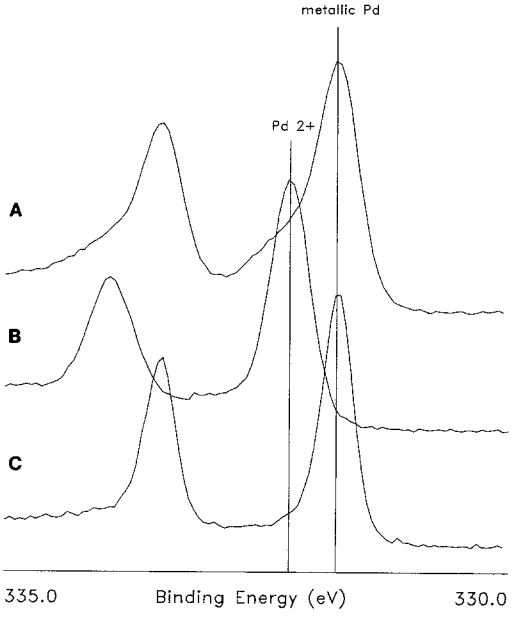

FIG. 1. XPS Pd 3*d* core-level spectra of sample 1 (A) as received, (B) after oxidation, and (C) after reduction.

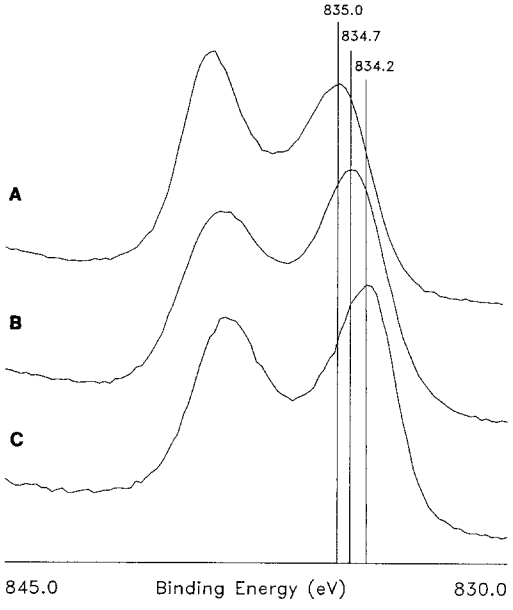

FIG. 2. XPS La 3*d* core-level spectra of sample 1 (A) as received, (B) after oxidation, and (C) after reduction.

core-level peak. This La spectrum is similar to that previously observed for lanthanum carbonate (*17*). After oxidation, the La binding energy was shifted down to 834.7 eV, 1.5 eV higher than expected for lanthanum oxide (*17*). We speculate from the elemental compositional data (not included) that the higher binding energy observed can be attributed to the formation of lanthanum sulfate. However, we cannot verify this speculation through the core level data, since due to the broad nature of the La 3*d* core level, it is not realistic to deconvolute the La 3*d* envelope and identify each chemical state. The La binding energy observed for the hydrogen-treated film was shifted down even further to 834.4 eV, which is still 1.2 eV above that of lanthana (833.2 eV). The shift is clearly in the direction opposite to that expected for reduction of La^{3+}. We assign this change tentatively to a reaction with the Cl impurity to form a lanthanum oxy-chloride species. The La spectrum (Fig. 2c) cannot be explained simply as a mixture of La_2O_3 and $LaCl_3$, since a standard powder of $LaCl_3$ was shown to exhibit an La binding energy of 835.1 eV and a satellite peak at twice the intensity of the core-level peak. These results do not negate the conclusion that prolonged *in situ* treatment by H_2 at 600°C yielded no reduction in the oxidation state of lanthana below +3.

An assessment of the hypothetical bulk reduction thermodynamics of trivalent lanthana to a divalent oxide at 900°K shows immediately its improbability. Thus, in $La_2O_3 + H_2 \rightleftarrows H_2O + 2LaO$, $\Delta F_{900°K}$ is respectively −366.9 (*20*) and −47.3 Kcal/mole for La_2O_3 and H_2O. Thus the energy of formation of bulk divalent lanthanum oxide under our conditions is more than +150 Kcal per mole of LaO. A vanishing trace of water in the gas phase would reoxidize the divalent oxide back to lanthana. One has to postulate an extremely unstable La^{3+} ion on the surface for it to be reducible. But as always such surface thermodynamic data are not available.

The data given in Table 2 show that initially for sample 2, where La was deposited last, a higher La/Pd ratio was observed. However, the ratios observed for samples 1 and 2 were similar after oxidation treatment, and did not change after the reductive treatment, implying that after the first treatment the films were well mixed.

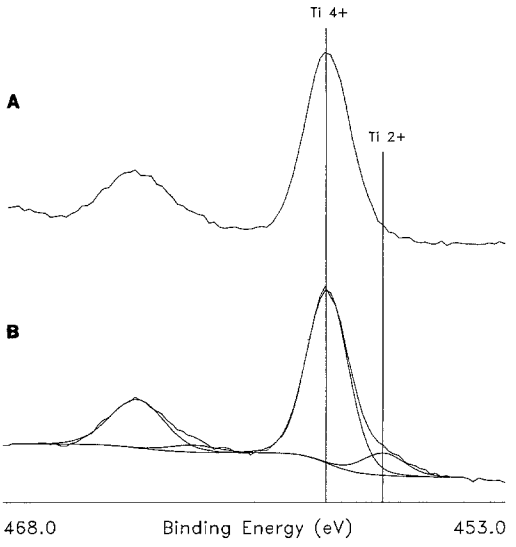

FIG. 3. XPS Ti 2*p* core-level spectra of sample 3 (A) after oxidation and (B) after reduction.

Ti-containing films. As was the case in the La/Pd films, with the Ti-containing films the binding energy of La corresponds always to the trivalent state. Pd is metallic under the reducing conditions and is observed as PdO after oxidizing conditions. The Ti 2*p* spectra acquired on the Ti/Pd binary film (sample 3, Table 1) after the oxidative and reductive treatments are given in Fig. 3. Figure 3a reveals a single Ti $2p_{3/2}$ centered at 458.4 eV which is normally attributed to Ti^{4+} (*21*). After the H_2 treatment (Fig. 3b), an additional peak is observed at 456.7 eV (labeled Ti 2+ in Fig. 3). Recently, Bardi (*22*) has summarized all the available information on the composition and structure of thin films of Ti oxides on Pt surfaces or in contact with Pt. A thin layer of TiO observed in these systems produced an XPS peak in the binding energy range of

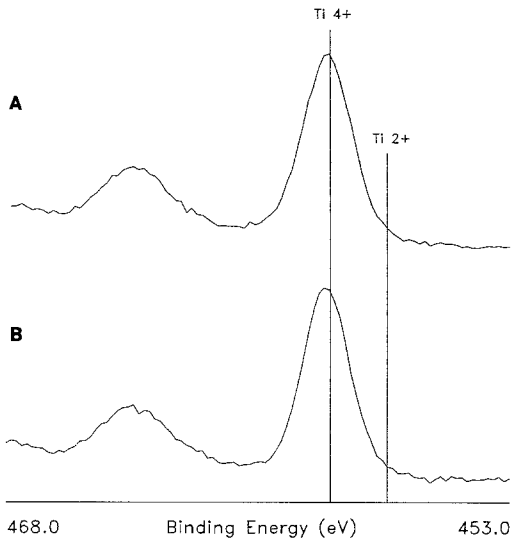

FIG. 4. XPS Ti 2*p* core-level spectra of (A) sample 4 and (B) sample 5 after reduction.

456.3–456.9 eV, which encompasses the lower binding energy Ti $2p_{3/2}$ peak in Fig. 3b. However, this binding energy value is not in agreement with energies reported for bulk TiO (454.8–455.3 eV) by Bardi (*22*) and others (*23*). Bardi rationalizes this discrepancy by hypothesizing a possible involvement of "Ti^{3+}" centers. These considerations, although of interest, are not essential in these studies. The reducibility observed in this work, can, however, be rationalized by assuming that thin films containing Ti and Pd oxides when submitted to reducing conditions produce a thin layer of TiO analogous to the thin layer of TiO on Pt as discussed by Bardi (*22*).

It has also been reported (*23*) that exposure of TiO_2 and Rh,Pt/TiO_2 to H_2 at 550°C did not produce any observable reduction of the titania. Obviously, under the conditions presented in our work (increased pressure and slightly increased temperature), reduction was accomplished. The difference may also result from the nature of the samples studied.

Figure 4 presents the Ti 2*p* spectra acquired on the Ti/Pd films incorporated with La (samples 4 and 5) after reduction. In both cases a single Ti $2p_{3/2}$ peak was present at a binding energy of 458.6 eV, nearly identical to that observed for Ti +4 in sample 3. The addition of lanthana to these films completely prevented the reduction of titania previously observed on the binary film of Ti and Pd without La (Fig. 3b). This inhibition of reduction occurred regardless of the deposition sequence or the amount of lanthana deposited.

Monitoring the La/Ti and La/Pd ratios (Table 2) reveals a substantial increase of the relative amount of La observed after oxidation and another increase after reduction treatments regardless of deposition sequence. These results suggest a covering or coating of the lanthana over the titania which impedes the reduction of the titania as observed in the high-resolution Ti 2*p* spectra (Figs. 4a and 4b).

Nb-containing films. The chemical states of La and Pd observed after oxidation and reduction treatments were the same as those observed in the Ti-containing films. The XPS Nb 3*d* core-level spectra of the binary film (sample 6, Table 1) after the oxidative and reductive procedures are presented in Fig. 5. The oxidized material reveals a single state of Nb (Fig. 5a) with the $3d_{5/2}$ peak centered at 206.8 eV, in good agreement with values reported for Nb_2O_5. The spectrum given in Fig. 5b reveals three separate states of Nb present after reduction. Spectral peaks were observed at 206.8, 205.3, and 203.5 eV, which can be attributed to Nb^{5+}, Nb^{4+}, and Nb^{2+}, respectively. These values are again in good agreement with those which have been previously reported (*21*). These results indicate that the Nb_2O_5 is more susceptible to reduction than the TiO_2. Table 3 summarizes the quantitative analyses attained from the computer peak fits of the Nb spectra acquired after the reductive treatments for the binary and two ternary films. Approximately half of the Nb in the binary film has been reduced to either +4 (26%) or +2 (20%).

Figure 6 presents the Nb 3*d* spectra of the reduced Nb/Pd films with the incorporation

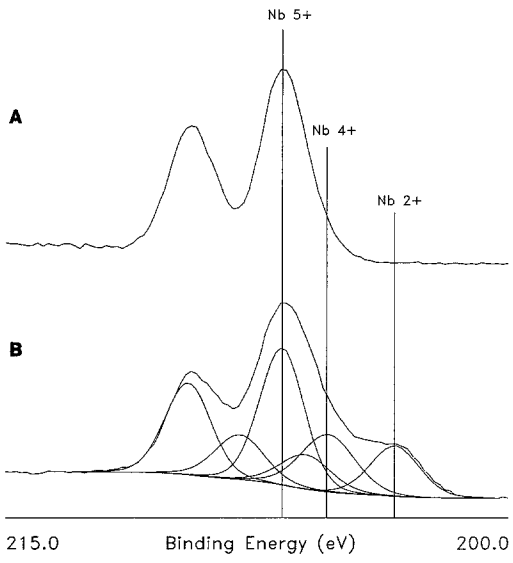

FIG. 5. XPS Nb 3*d* core-level spectra of sample 6 (A) after oxidation and (B) after reduction.

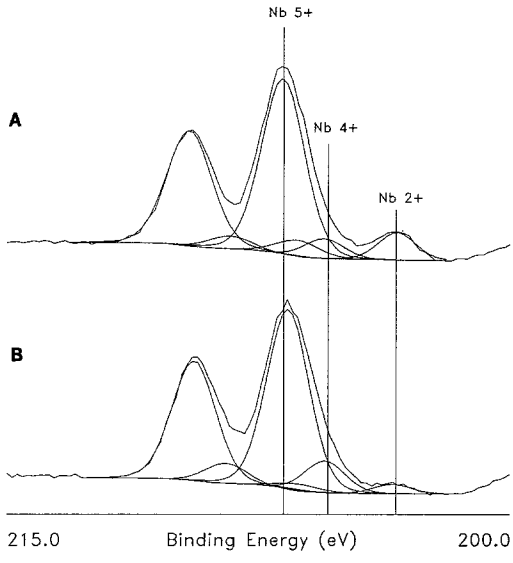

FIG. 6. XPS Nb 3*d* core-level spectra of (A) sample 7 and (B) sample 8 after reduction.

of La. As with the binary film, three Nb $3d_{5/2}$ peaks were observed, at essentially the same binding energies, attributable to Nb^{5+}, Nb^{4+}, and Nb^{2+}. Although qualitatively the same reduced states of Nb (+4 and +2) are observed on both ternary films as was observed on the binary film, the intensity of these peaks in the presence of La with respect to the Nb^{5+} peak decreased considerably. The quantitative results acquired from the Nb 3*d* spectral fits supporting these observations are given in Table 3. The spectra portrayed in Fig. 6 and the results given in Table 3 reveal that although a decrease in the amount of Nb reduction was observed in the presence of La, total suppression of reduction as observed on the Ti/Pd/La films did not occur under the same reactor conditions. In addition, Table 3 also reveals differences in the relative ratio of Nb^{4+} and Nb^{2+} in the ternary films. This may have resulted from either the difference in the position of the La layer (Nb/La/Pd versus La/Pd/Nb) or the difference in the thickness of the La layer (10 vs 5 Å).

TABLE 3

Nb Valence States after Reduction at 600°C

Sample	Nb valence states (%)		
	+5	+4	+2
6 (10 Å NbO_x/5 Å Pd)	54	26	20
7 (5 Å NbO_x/5 Å La/5 Å Pd)	80	9	11
8 (10 Å La/5 Å Pd/5 Å NbO_x)	82	15	3

The XPS La/Nb and La/Pd atomic ratios for the Nb containing films are given in Table 2. As previously discussed for the Ti-containing films, a substantial increase in the La/Ti and La/Pd ratios was observed after each treatment. However, in the case of Nb this was only observed in the La/Pd ratios. Although the La/Nb ratios in Table 2 increased after oxidation, no appreciable increase was observed on either of the Nb/Pd/La materials after reduction. These results suggest that the limited Nb reduction observed in Fig. 6 compared to the lack of Ti reduction observed in Fig. 4 may be explained by the extent of lanthana coverage on these respective metal oxides. Attempts were made to further corroborate these ob-

servations by establishing preferential association of the lanthana with niobia/titania through SEM and SAM/AES analyses, however, this was not observed within the spatial resolutions achievable with these techniques.

The ability of lanthana to retard the reduction of either niobia or titania is well proven by comparison of the respective binary and ternary films after reduction. Explanation of the complete suppression of reduction in the Ti systems compared with only decreased reduction of the Nb systems can be twofold: (1) the limited coverage of the lanthana on the niobia compared to titania may have resulted in less suppression of reduction and (2) the greater reducibility of niobia as seen in the comparison of Figs. 1b and 2b. It is also important to re-emphasize that before and after *all* treatments on *all* the films containing La, the oxidation state of La remained constant (trivalent), with no observable reduction.

Ce-containing films. As was the case in for the previous films, after treatment in H_2 at 600°C the binding energy of La remains in the trivalent state in each of the Ce films, further confirming its irreducibility. Pd is metallic under the reducing conditions and is observed at 337.1 ± 0.1 eV after oxidizing conditions. This value is about 0.5 eV higher than that observed for a reference PdO foil, and in thin films consisting of Pd on sapphire in the presence of La (samples 1 and 2), Ti, Ti/La, Nb, and Nb/La (samples 3–8). The slightly higher Pd binding energy noted here, always in the presence of Ce, implies the possibility of a Pd interaction with fully oxidized ceria which is stronger than that with the other investigated oxides. Using other examination techniques Sass *et al.* (*24*) have established that in the presence of ceria the reduction of Pd^{2+} is attenuated. The aim of this work, however, is to determine the reducibility of ceria in the presence of lanthana and lanthana plus γ-Al_2O_3 and therefore this effect merits no further discussion.

Interpretation of the Ce 3*d* core-level spectra acquired from these films proved extremely difficult when mixed oxidation states were present (Ce^{3+}, Ce^{4+}). However, work originating from this laboratory by Shyu *et al.* (*25–27*) has shown that the reducibility of ceria, from Ce^{4+} to Ce^{3+}, can be monitored by following an unobscured peak, designated as u''', in the complex XPS cerium oxide spectra. The $u'''(v''')$ peak, observed only when ceria is present in the +4 state, is attributed to the portion of the transitions to the final state $4f^0$ from the initial state $4f^0$ which accompany the Ce $3d_{3/2}$ ($3d_{5/2}$) photoemission process (*28*). Shyu *et al.* established (*26, 27*) that the fraction of the total Ce signal in the u''' peak and the extent of the degree of oxidation vary linearly, allowing one to establish the latter from measurement of the former. Following this methodology, we use the u''' satellite peak, at the binding energy of 916.5 eV, to determine the extent of Ce^{4+} reduction. Table 4 summarizes the calculated fraction of the Ce signal attributable to u''', and thus the amount of Ce^{4+}, for the various samples and treatments discussed in the following Ce-containing films.

TABLE 4

Amount of Ce in +4 State for Various Samples and Treatments

	Sample	%u''' (% Ce^{4+}) treatment	
		H_2 600°C	O_2 600°C
9	(10 Å CeO_x/5 Å Pd)	0.0 (0)	13.4 (100)
10	(10 Å CeO_x/5 Å Pd/5 Å La)	2.7 (20)	13.9
11	(10 Å CeO_x/5 Å Pd/10 Å La)	2.6 (19)	14.3
12	(10 Å CeO_x/5 Å Pd/20 Å La)	2.8 (21)	14.8
13	(γ-Al_2O_3/10 Å CeO_x/5 Å Pd/10 Å La)	0.6 (4.5)	
14	(γ-Al_2O_3/10 Å CeO_x/5 Å Pd/20 Å La)	0.7 (5.2)	

The XPS spectra of cerium acquired from the binary film (sample 9) after oxidation and reduction are presented in Fig. 7. The fraction of the total Ce signal attributable to the u''' peak in the oxidized sample is 13.4%, exactly the same as in pure fully oxidized ceria (Ref. (*25*), Table V). The u''' peak is absent in the XPS spectrum of the reduced

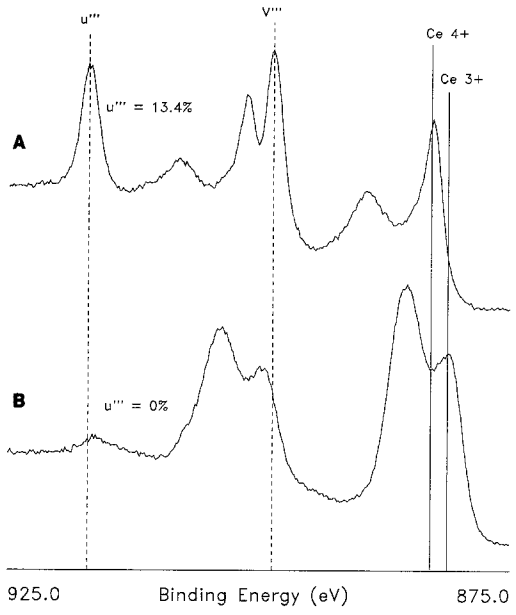

FIG. 7. XPS Ce 3*d* core-level spectra of sample 9 (A) after oxidation and (B) after reduction.

film. Thus, the ceria in the film undergoes a complete, 100% reduction from the tetravalent to the trivalent state when changing the atmosphere from pure O_2 to pure H_2 at 600°C. A small and broad signal which resided in the vicinity of u''' in the reduced film, associated with the $3d_{3/2}$ core level of Ce^{3+}, was also apparent for the $3d_{5/2}$ core level in between the $3d_{5/2}$ and $3d_{3/2}$ regions in Fig. 7b. The calculation of u''' in all Ce 3*d* spectra (Figs. 7–10, summarized in Table 4) was corrected for this peak.

Figure 8 indicates that with the addition of lanthana, not all the ceria in the sample is reduced. Irrespective of the amount of lanthana, (2.7/13.4 (u''' reduced/u''' oxidized)) × 100 or approximately 20% remains oxidized, even at the very drastic reduction conditions. The reoxidation shown in Fig. 9 is complete. We ascribe the somewhat higher u'''-character measured in the samples with La to the higher noise level present in the Ce 3*d* spectra (compare the La/Ce-oxide ratios given in Table 2). The spectral noise level increased as the Ce signal diminished, introducing an error associated with the integration of the u''' peak.

The introduction of lanthana did not completely hamper the oxyreduction of the ceria. Clearly, in our case, it does not inhibit at all the reoxidation of partially reduced films, and it inhibits the reduction only partially. Qualitatively, though, the results are congruent with those observed for titania and niobia. Interestingly enough, the fourfold increase in the thickness of the La layer did not increase the shielding of the ceria.

The presence of a γ-Al_2O_3 layer in the film affords an almost complete reduction (Fig. 10). Instead of 20% in its absence remaining in the oxidized form, only (0.65/13.4) × 100 or approximately 5% of the ceria in the film is not accessible to reduction. This points to the redistribution of La into the γ-Al_2O_3 layer, as confirmed in the corresponding data given in Table 2, where a lower La/Ce ratio was observed compared to those films where the γ-Al_2O_3 coating was absent.

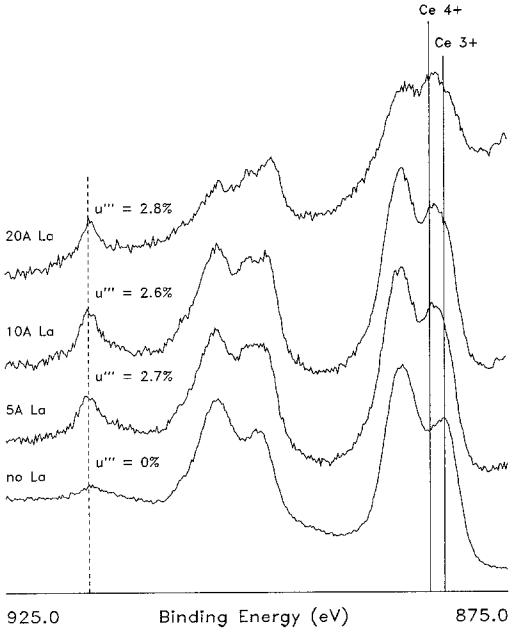

FIG. 8. XPS Ce 3*d* core-level spectra of reduced samples 9, 10, 11, and 12; films without a γ-alumina layer.

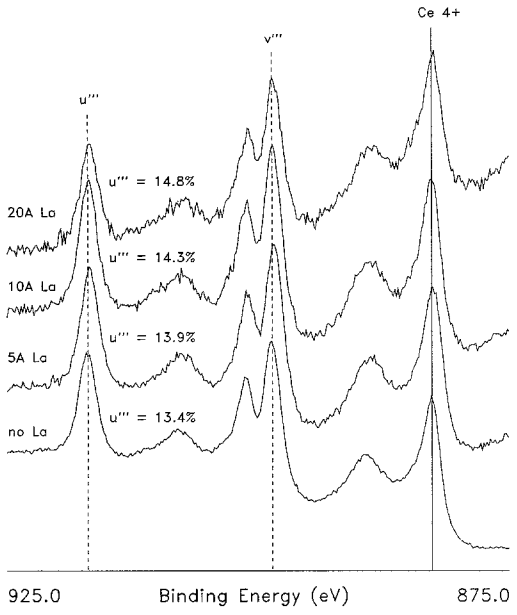

FIG. 9. XPS Ce 3*d* core-level spectra of oxidized samples 9, 10, 11, and 12; films without a γ-alumina layer.

As similarly noted for the Ce containing films applied directly onto sapphire, the uncovering of the shielded part of the ceria by the γ-Al_2O_3 layer did not depend on the thickness of the lanthana deposit. It is not worthwhile to speculate about the reasons since the detailed morphology and the degree of interpenetration of the film ingredients is unknown to us. Nevertheless, under our experimental conditions, the presence of lanthana shields ceria (partially) from reduction and the introduction of γ-Al_2O_3 causes lanthana redistribution in a way that virtually nullifies this shielding.

CONCLUSIONS

XPS characterization of thin films containing lanthana, with and without the presence of oxides possessing multiple oxidation states, revealed that no change in the original oxidation state of lanthana (+3) occurred after being subjected to prolonged *in situ* H_2 reduction at 600°C. The binding energy of the La $3d_{5/2}$ peak envelope appeared at an elevated value in comparison to that observed for pure La_2O_3 regardless of the presence of Pd.

It is our finding that the presence of valence-invariant lanthana, impedes the reducibility of oxides such as Ti, Nb, and Ce. That lanthana interacts with the surface of nonreducible oxides such as alumina has been demonstrated previously by work from our laboratory (*29*). In the same systems, the reducibility of precious metal such as Pd is unaffected. Furthermore, the degree of reduction of the reducible oxides is governed by the degree of contact of the valence-invariant rare earth oxide with the reducible oxide and/or the reducibility of the later.

The present work highlights the relevance of the study of model systems to practical catalysis. Since γ-alumina, ceria, noble metals, and presently lanthana are important ingredients in modern automotive catalysts, the understanding of their mutual interactions, accessible in model systems such as described here, is of substantial and immedi-

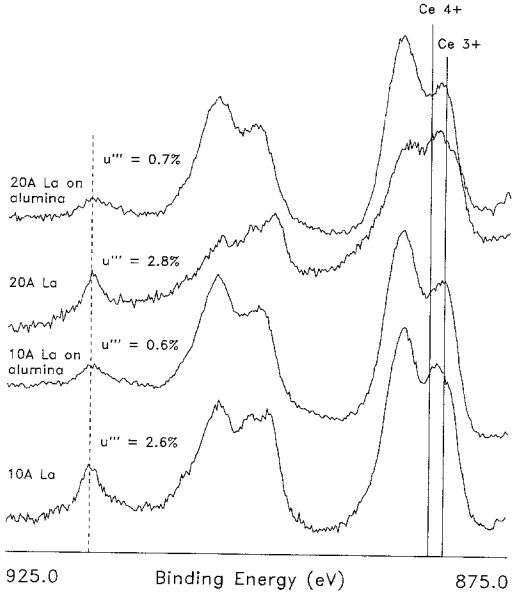

FIG. 10. XPS Ce 3*d* core-level spectra of reduced samples 11, 13, 12, and 14; films with and without a γ-alumina layer.

ate importance in the continuing quest to improve the performance of these catalysts.

ACKNOWLEDGMENTS

Max Bettman (now retired) spurred us on to look for firm evidence of the surface reducibility of lanthana (or otherwise). P. Schmitz and G. Graham freely shared their expertise in surface studies. We thank R. Liu for SEM examination and R. Chase for SAM/AES investigation of these samples. C. Narula helped in the deposition of the γ-Al_2O_3 layer on sapphire slides.

REFERENCES

1. Tauster, S. J., *Acc. Chem. Res.* **20,** 389 (1987).
2. Smith, D. W., *J. Chem. Educ.* **63,** 228 (1986).
3. Moeller, T., *in* "Comprehensive Inorganic Chemistry" (J. C. Bailar *et al.*, Eds.), Vol. 3, p. 1 ff, Pergamon, New York, 1973.
4. Tauster, S. J., Fung, S. C., Baker, R. T. K., and Horsley, J. A., *Science* **211,** 1121 (1981).
5. Rieck, J. S., and Bell, A. T., *J. Catal.* **99,** 262 (1986).
6. Muraki, H., Shinjoh, H., Sobukawa, H., Yokota, K., and Fujitani, Y., *Ind. Eng. Chem. Prod. Res. Dev.* **25,** 202 (1986).
7. Muraki, H., Shinjoh, H., and Fujitani, Y., *Appl. Catal.* **22,** 325 (1986).
8. Ryndin, Yu. A., Hicks, R. F., Bell, A. T., and Yermakov, Yu. I., *J. Catal.* **70,** 287 (1981).
9. Campbell, K. D., Zang, H., and Lunsford, J. H., *in* "Proceedings (and preprint C-5), 10th North-American Catalysis Society Meeting, San Diego, CA, May 17–22, 1987."
10. "Gmelin Handbuch Der Anorganischen Chemie," 8th ed., System No. 39, Vol. C1, p. 177ff., Springer-Verlag, Berlin/New York, 1974.
11. Ref. (*10*), p. 205.
12. Gandhi, H. S., Piken, A. G., Shelef, M., and Delosh, R. G., Paper No. 760201, Society of Automotive Engineers, Warrendale, PA, 1976.
13. Yao, H. C., and Yu Yao, Yu. F., *J. Catal.* **86,** 254 (1986).
14. Harrison, B., Diwell, A. F., and Hallett, C., *Platinum Met. Rev.* **32**(2), 72 (1988).
15. Engler, B., Koberstein, E. and Schubert, D., *Appl. Catal.* **48,** 71 (1989).
16. Miki, T., Ogawa, T., Haneda, M., Kakuta, N., Ueno, A., Tateishi, S., Matsuura, S., and Sato, M., *J. Phys. Chem.* **94,** 6464 (1990).
17. Haack, L. P., deVries, J. E., Otto, K. and Chattha, M. S., *Appl. Catal.* **82,** 199 (1992).
18. Bryson, C. E., III, *Surf. Sci.* **50,** 189 (1987).
19. Otto, K., Haack, L. P., and deVries, J. E., *Appl. Catal.* (B) **1,** 1 (1992).
20. Sharupin, B. N., and Vasil'kova, I. V., *J. Gen. Chem. U.S.S.R.* (*Engl. Transl.*) **31,** 1941 (1961), cited from Ref. (*10*), p. 209.
21. "Handbook of X-ray Photoelectron Spectroscopy," 1st ed., Perkin–Elmer Corporation, Physical Electronics Division, 1979.
22. Bardi, U., *Catal. Lett.* **5,** 81 (1990).
23. Sexton, B. A., Hughes, A. E., and Foger, V., *J. Catal.* **77,** 85 (1982).
24. Sass, A. S., Kuznetsov, A. V., Shvets, V. A., Savel'eva, G. A., Popova, N. M. and Kazanskii, V. B., *Kinet. Katal.* (*Engl. Transl.*) **26**(6), 1217 (1985).
25. Shyu, J. Z., Weber, W. H., and Gandhi, H. S., *J. Phys. Chem.* **92,** 4964 (1988).
26. Shyu, J. Z., Otto, K., Watkins, W. L. H., Graham, G. W., Belitz, R. K., and Gandhi, H. S., *J. Catal.* **114,** 23 (1988).
27. Shyu, J. Z., and Otto, K., *J. Catal.* **115,** 16 (1989).
28. Fujimori, A. J., *Magn. Magn. Mater.* **47, 48,** 243 (1985).
29. Bettman, M., Chase, R. E., Otto, K., and Weber, W. H., *J. Catal.* **117,** 447 (1989).